POLITECNICO DI TORINO
Repository ISTITUZIONALE

Electrochemical Evaluation of Human Hair Derived Carbon Particles

(Article begins on next page)

17 October 2023

Graphical Abstract
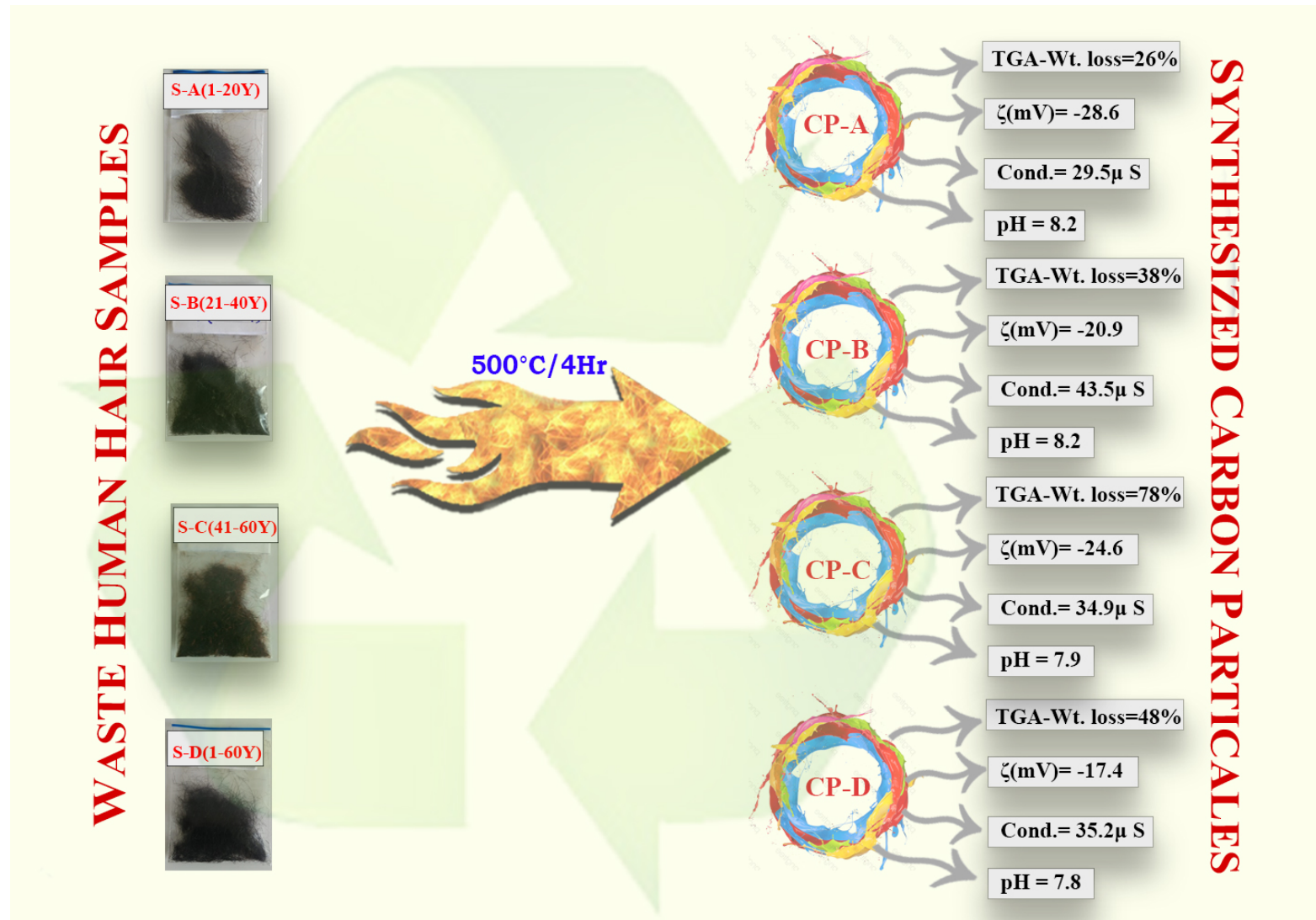
ELECTROCHEMICAL EVALUATION OF HUMAN HAIR DERIVED CARBON PARTICLES

Muhammad Atif [*-1-2], Muhammad Qamar Farid [-1], Sheikh Asrar Ahmad[1], Ramzan Abdul Karim[3], Muhammad Azhar [4], Faiz Rabbani [5], Roberta Bongiovanni [2]

[1] Department of Chemistry, University of Education Lahore - Vehari campus, Vehari, Punjab, Pakistan.
[2] DISAT, Politecnico Di Torino, Corso Duca Degli Abruzzi-24, Torino-10129, Italy
[3] Faculty of Material and Chemical Engineering, GIKI, KPK, Pakistan.
[4] University of Engineering and Technology, Wah, KPK, Pakistan.
[5] Department of Environmental Sciences, COMSATS, Vehari, Punjab, Pakistan.

Abstract

Pollution has become a great challenge for modern world. Hence, recycling trend is growing worldwide. Human hair, a fancy part of human body, creates a bulk of litter on trimming, yet has wide spectrum of applications. A facile thermal approach has been implemented in this research to synthesize carbon particles (CP) from waste human hair. CP surface analyses was made through SEM, ATR-FTIR, TGA & Raman. Efficient adsorptive behavior of synthesized CP against Zn and Pb has been observed with 70% Pb (9.325mg/10mg CP) and 90% Zn (37mg/10mg CP) adsorption. The augmented adsorptive capacity of CP ultimately finds its application in heavy metal removal from waste water. Cyclic voltammetry (CV) justified outstanding adsorption behavior of CP by speedy electron transfer, better charge storage and swift ionic diffusion; with 53 mC current carrying capacity and 1.98 to 4.37 cm^2 effective surface area. CV data has shown electrochemical irreversibility and double layer capacitance. CP conductivity has been observed from 19.78 µS to 38.4 µS, with ζ values between -17.4 mV and -28.6 mV.

Keywords: Human Hair Waste Recycling; Energy Storage; Carbon Particles; Electrochemical behavior; Heavy Metal Adsorption;

[-] Share first authorship

[*] Dr. Muhammad Atif, Department of Chemistry, DS&T,
University of Education Lahore (Vehari Campus), Punjab, Pakistan.
Cell: +92 3024757979
Email: chemistatif@yahoo.com , muhammad.atif@ue.edu.pk

1. INTRODUCTION

Human hair is an accessory of vertebrate skin that makes appealing look of personality. When this filamentous extension is treated by hairdresser, turns into waste material which becomes the part of environmental pollution. Human hair as per its chemical composition i.e 51% C, 17% N, 21% O along with 6% H and 5% S, has been a source of material with electrochemical response [1-6]. Although its composition changes with some factors like age [7] and environment [8], yet, human hair holds special features like high tensile strength, reduced decomposition, good thermal insulation, elasticity and above all ability to interact with both oils and water. All these characters have defined a broad spectrum of human hair applications [9].

Recycled material from waste human hair carries electrochemical properties established on the fact that decomposition of human hair gives C, S, N and heteroatoms usually used in doped supercapacitors [10-13]. Conductive behavior of human hair derived CP has been observed to be exceptional as compared to other allotropes of carbon [14-18].

Current research is based on a facile thermal approach of CP synthesis from waste human hair, characterized for their excellent adsorptive behavior and electrochemical performance. These findings suggest the use of prepared CP not only in renewable energy resources but also in heavy metal removal from waste water.

2. EXPERIMENTAL

2.1 Material

Human hair sampling was done from different commercial areas of Vehari (Punjab, Pakistan). Collected samples were classified into four main types, S-A, S-B, S-C, S-D (detail in Table 1). Nitrogen gas was used to avoid over-oxidation. HCl (37% pure, density 1.19g/ml, Sigma Aldrich), Calcium Carbonate (BDH Laboratory), Ethylenediamine tetraacetic acid (EDTA 0.01M, Sigma-Aldrich, mol. Wt. 372.24 g/mol, density 860kg/m^3), Ammonium Chloride, Eriochrome Black T (EBT), Phenolphthalein were used during characterization. Standard

metal solutions (0.1M) of Pb and Zn were used to study heavy metal adsorption on CP. All chemicals used in experimentation were of analytical grade.

Table 1: Human Hair Samples

Sr #	Sample ID	Age of sampling population (Years)
1	S-A	1-20
2	S-B	21-40
3	S-C	41-60
4	S-D	S-A+S-B+S-C (Equal wt.)

2.2 CP Preparation

Collected hair samples were shampooed, rinsed with deionized water and dried at 65^0C for 4 hours. After drying the samples were cut by scissor into ≈ 4-5mm size. Weighed amount of pre-treated samples was taken into crucibles with lid, Nitrogen was inserted in crucibles with the help of syringe. Samples were heated for four hours at 500^oC. Human hair derived CP were synthesized in seven laps of temperature increment ($31-80^o$C, $80-150^o$C, $151-174^o$C, $175-210^o$C, $211-300^o$C, $301-400^o$C & $401-500^o$C). The laps in temperature increment were made to enhance carbonization process.
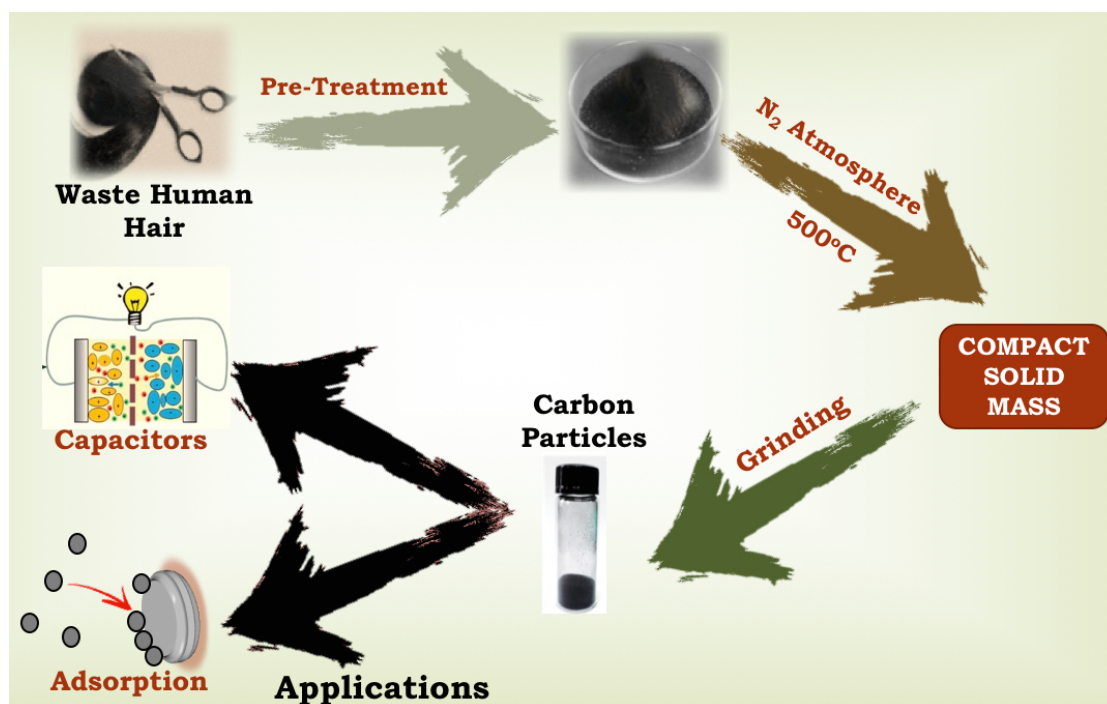

Figure 1: Preparation of CP

The obtained products were crushed with pestle mortar and stored in air tight plastic jars, as S-A, S-B, S-C and S-D respectively.

2.3 Metal Adsorption Analysis

Weighed amount of prepared CP were placed in 0.1M metal solutions for 24 hrs with constant stirring at room temperature. Then after 24 hrs, each solution was tested for remaining metal concentration, to picture the adsorbed metal concentration on CP.

2.4 Electrode Preparation Method for CV Analysis

Each CP (0.5 mg) was dispersed in dichloroethane for 10 minutes, deposited on electrode tip with optical cement and dried in open air for 2 hours. CV analysis of these CP coated electrodes was done in 1M NaOH with three electrode systems i.e. saturated calomel electrode (SCE as reference electrode), Pt electrode (counter electrode) and CP coated electrode (working electrode). CV curves were analyzed by "Echem analyst".

3. CHARACTERIZATION

CP have been analyzed through instrumental as well as chemical analyses. Functional group detection was done by FTIR equipped with Attenuated Total Reflectance (ATR) on CP by using ALPHA-P Broker absorbance spectra (4000–500 cm^{-1}). Surface morphology of CP has been observed through Scanning Electron Microscope (SEM; TESCAN VEGA3). Thermal stability of CP from 25°C to 800°C has been tested in Thermogravimetric Analysis (TGA; LIBRA F1 Netzsch Germany). CP structural evaluation has also been done by Raman spectroscopy (Renishaw Ramascope, Ar+ laser 514.5 nm excitation). Electrochemical behavior of CP has been tested through Cyclic Voltammetry (CV potentiostat, Gamry G-720). CV curves have been analyzed by "Echem analyst" to integrate peak areas. Zeta potential values have been tested by using Zeta Potential Potentiostat (Gamry G-720), by dispersing 1 mg CP in 100 mL deionized water and sonicated for 10 min before analysis.

4. RESULTS AND DISCUSSION

CP prepared from waste human hair through facile thermal approach have been evaluated for structural parameters (surface chemistry and morphology) through different instruments.
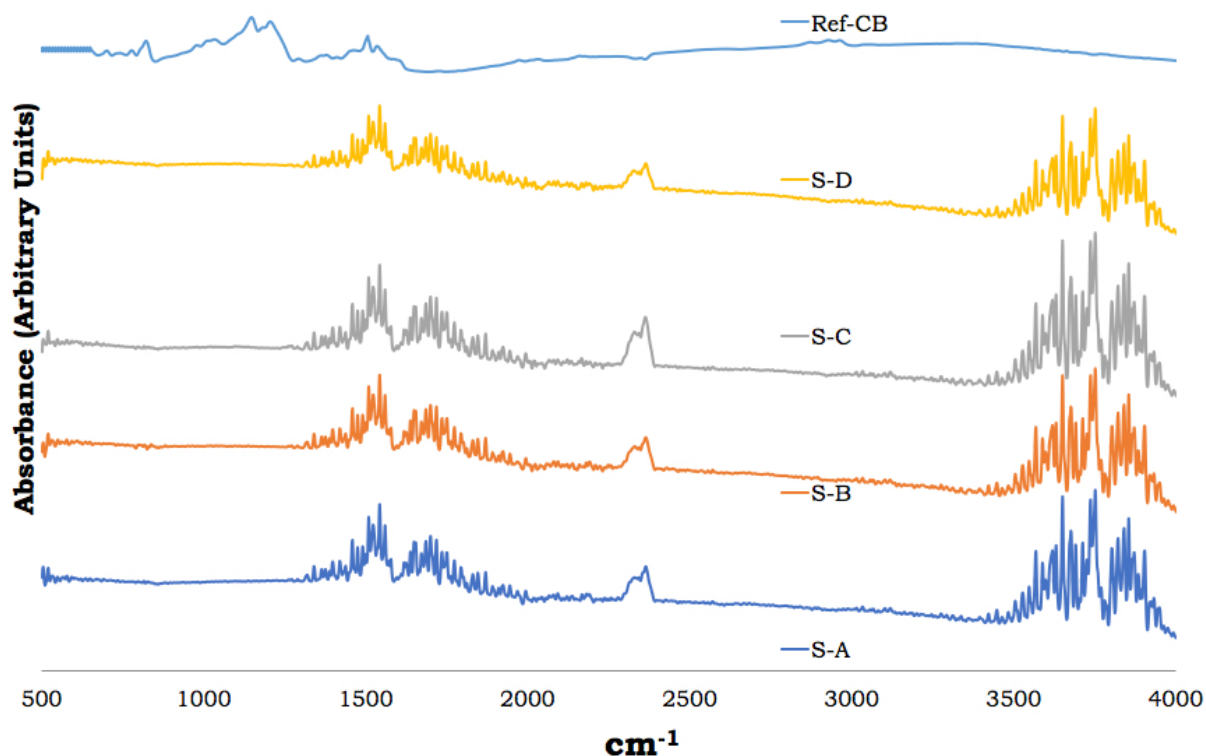

Figure 2: ATR-FTIR Absorbance Spectra of CP

CP samples, prepared from human hair, in solid form were analyzed through ATR-FTIR (Figure 2). Absorbance spectra were taken from 500 to 4000 cm^{-1}. All the samples showed five sets of very prominent peaks. Two peak sets at ~1540 cm^{-1} and ~1660 cm^{-1} have been appointed as C-C and C-O bond stretching [13, 19]. A notably sharp peak has been spotted at ~2215 cm^{-1} for CO_2 bond stretching [14] and relatively stronger absorption peaks at ~3660 cm^{-1} and ~3760 cm^{-1} for N-H stretching of NHR_2 and O-H stretching of alcohol [13,19], respectively. Moderately developed peak intensities of CP prepared from sample S-C confirm presence of functional groups on their surface.
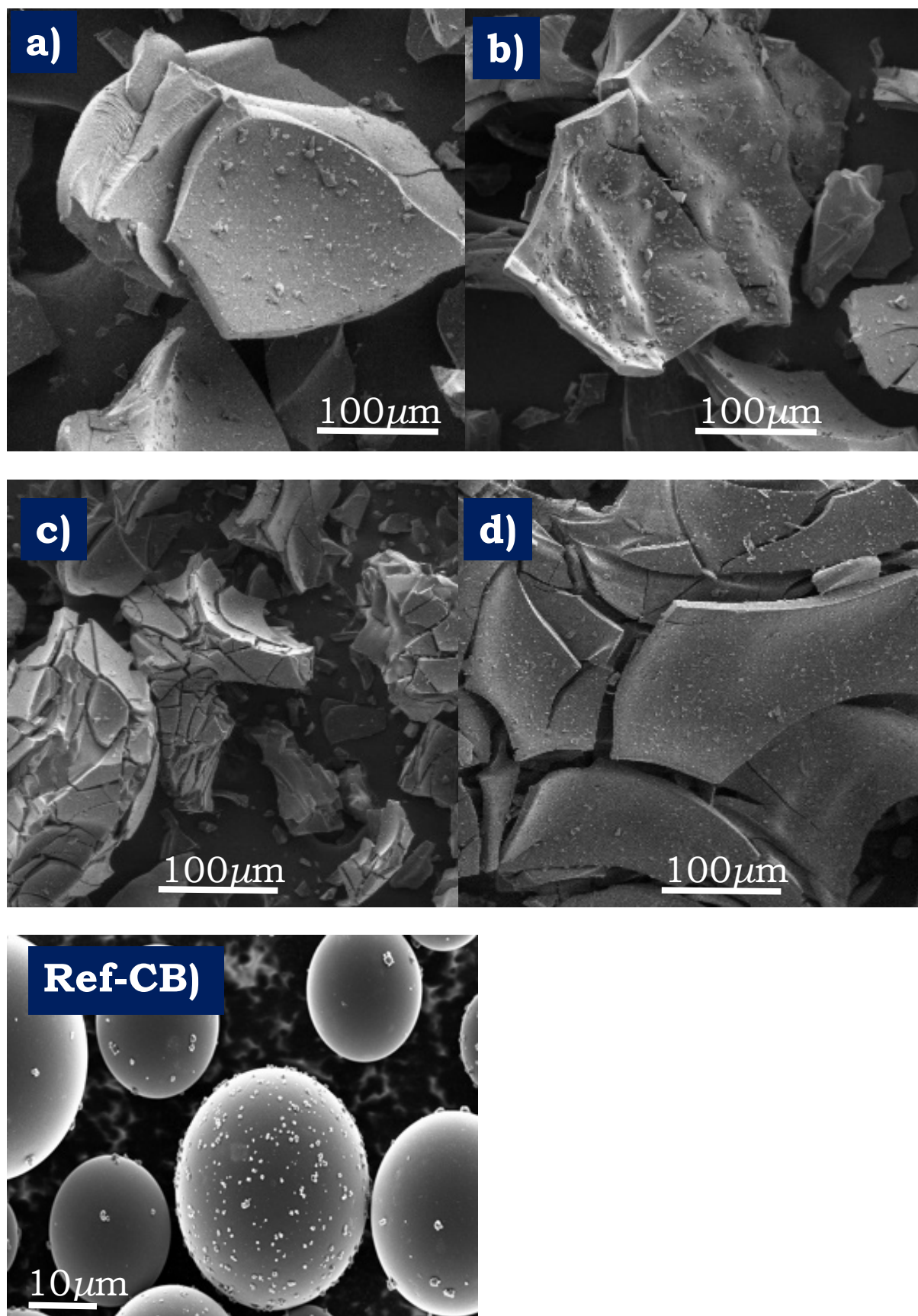
Figure 3: SEM images of CP a) S-A, b) S-B, c) S-C, d) S-D, e) Ref-CB

Morphology of prepared CP, have been observed through SEM (Figure 3 a-d). For all the samples, granular appearance with layered structure has been found indicating no marked difference in morphology for samples S-A, S-B and S-D, however sample S-C has been found with smaller granular structure. Crystallite size calculated through Raman Analysis (Table 3) has been found almost same for all the samples. Comparatively S-B has been found with slightly higher value of 4.73 nm. SEM image of commercial carbon black (CB) has also been presented for comparative study.

SEM images were taken to compare morphology and particle size of all prepared samples, which have been found equivalent for three samples except S-C. Morphology and particle size defines the stability of CP dispersion in liquid medium; stable the dispersion better adsorption/conduction properties in solution or composites.
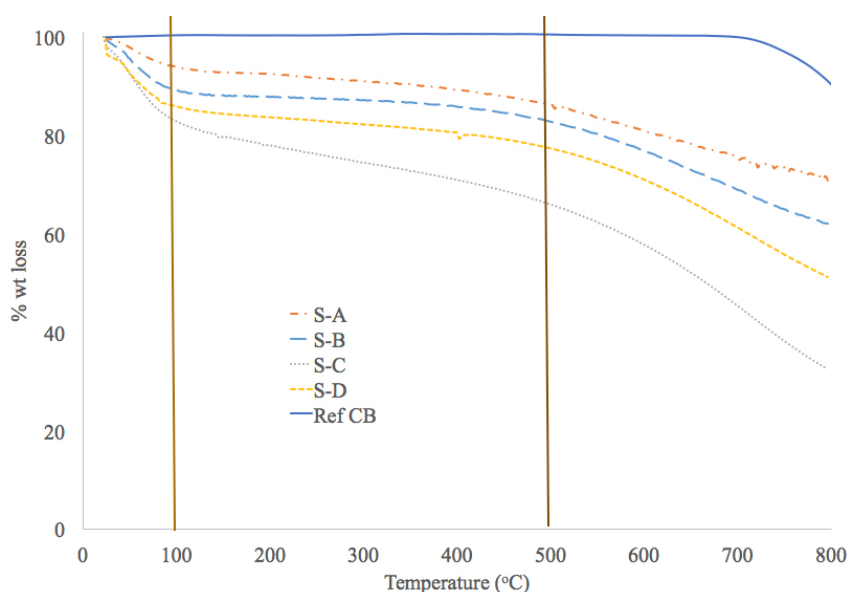
Figure 4: TGA for CP from 25°C to 800°C of: **a)** S-A **b)** S-B **c)** S-C **d)** S-D and Ref-CB

Table 2: Comparison of % wt. loss of CP samples

	Temperature	Ref-CB	S-A	S-B	S-C	S-D
% wt. loss of sample	25-100°C	0	7	12	18	15
	101-500°C	0	7	9	14	7
	501-800°C	10	15	17	33	26
Total %wt. loss	**25-800°C**	**10**	**29**	**38**	**65**	**48**

Thermal decomposition behavior of all prepared samples was studied through TGA (Fig 4). For the purpose, each sample (0.03g) was taken in ceramic pan and exposed to heat ranging from 25 to 800°C, with an increment of 10°C/min. Obtained curves were divided into three segments to study the decomposition rate with respect to temperature (Table 2). Decomposition percentage in first segment (25-100°C) for S-A, S-B, S-C and S-D has been found to be 7%, 12%, 18% and 15% respectively. This decomposition segment may be attributed to the evaporation of volatile or physically adsorbed moisture/gases on CP surface, as reported in literature [14]. In second segment (101-500°C) better thermal stability has been observed in all samples. Comparatively sample S-C has shown higher decomposition (14%), almost double than others($\cong$7%). The thermal instability of S-C may be attributed to several factors including comparatively smaller particle size and/or greater quantity of oxidizable species on exposed surfaces of CP (FTIR data Fig 2). In the third segment of TGA curves (501-800°C) maximum decomposition for all CP has been observed. Upon comparison of total weight loss by the CP, sample S-C has shown highest decomposition (i.e. 65%), specifying extra oxidizable species on particle surface.
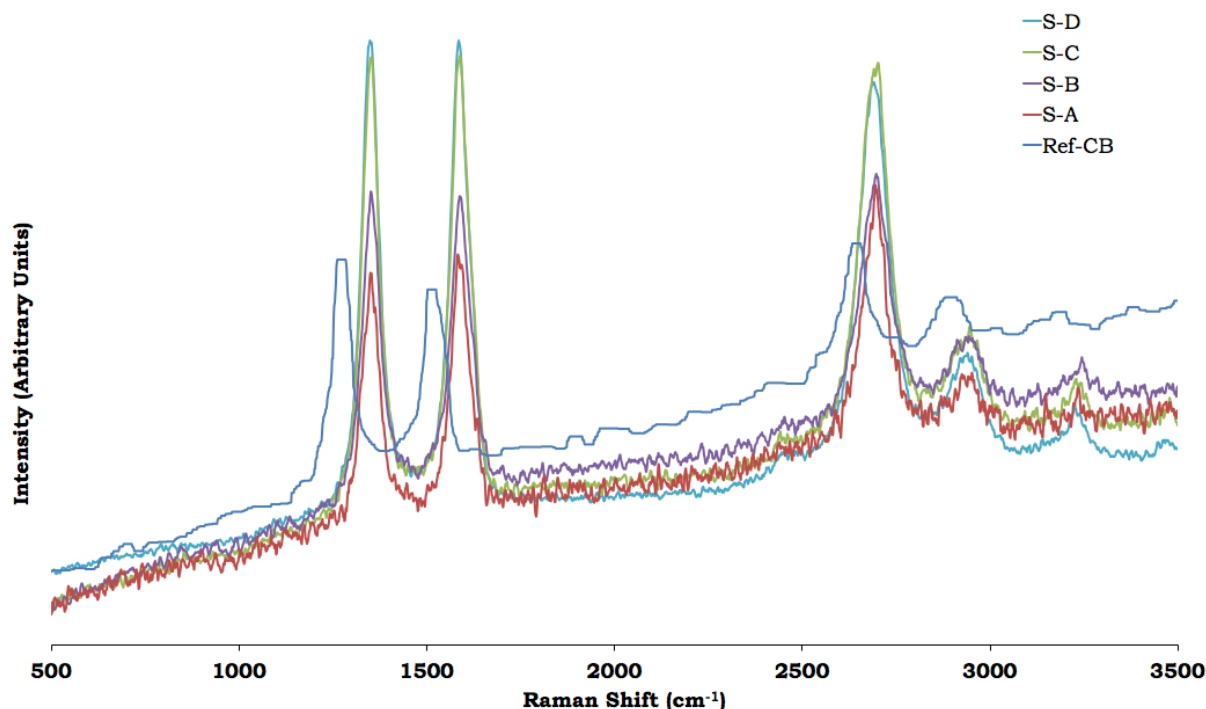
Figure 5: Raman analysis of prepared CP

Prepared CP samples have been evaluated through Raman (Ar+ laser 514.5 nm) for average crystallite size, which has been calculated through Tuinstra and Koenig formula [20] to evaluate L_a (lateral size of the crystallites).

$$L_a = 4.35\{Ig/Id\} \text{ nm} \quad ----- (i)$$

This estimation has been done through comparison of D peak at 1345 cm^{-1} representing disordered fragment and G peak at 1575 cm^{-1} representing graphitic fragment. There are two factors in Raman analysis that describe the crystallite size, i.e. peak width and peak intensity. Narrow peaks indicate larger crystallite size, since all the samples show similar peak width, therefore ratio of intensity of G and D peaks (I_G and I_D, respectively) is the only important parameter for determination of crystallite size as per Tuinstra and Koenig formula [20]. Figure 5 shows minute differences in the quoted characters. That is why, almost similar values for all samples (Table 3) have been observed. The information refers to primary particle (crystallite) size which, frequently blend into aggregates and subsequently to micro sized agglomerates.

Table 3: Raman Analysis data of prepared CP

Sample ID	I_G	I_D	L_a (nm)*

S-A	277	295	4.63
S-B	343	373	4.73
S-C	444	448	4.39
S-D	460	462	4.37

* calculated with equation (i)

Cyclic voltammograms of CP prepared from human hair are shown in Figure 6, along with a commercial glassy CB (Ref CB).
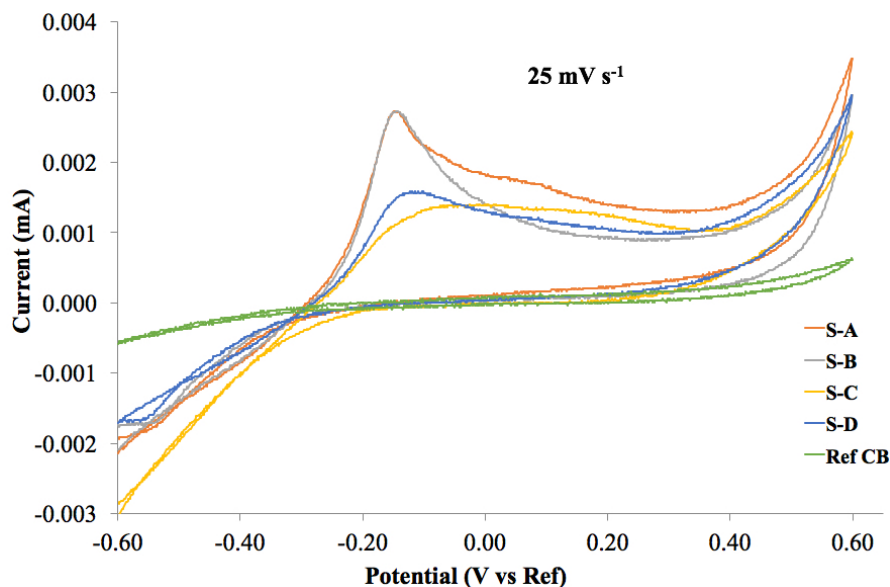

Figure 6: CV curves for CP at scan rate of 25mV/s in voltage range from -0.6 to 0.6 V in 1M NaOH solution

CV of prepared samples has been conducted to investigate the influence of surface chemistry in conductive performance of CP. Material's electrochemical stability has been observed in the range of potential from -600 to 600 mV at a scan rate of 25mV/s in 1M NaOH solution. CV comparison exposed augmented capacitance of CP than Ref-CB. A prominent anodic peak at about -200 mV and minute cathodic peak in voltammograms of samples S-A & S-B demonstrates electrochemical irreversibility, indicating fast electron transfer at the electrode surface compared to mass transport, suggesting a potential use of CP in renewable energy tools [21]. S-C and S-D sample curves in the graph (Fig 6) have quasi-rectangular shapes within potential window of -200 to 400 mV indicating the phenomena of double layer capacitance [22].

In figure 6, an enhanced current level, at lower potential, has been observed in samples S-A,

S-B and S-D, whereas in sample S-C the redox peak has shifted to higher voltage with reduced peak intensity and increased area under the peak, indicating enhanced ion diffusion at electrode-electrolyte interface [14] and augmented capacitance, respectively. Increase in area under cyclic voltammograms is interesting aspect in the development of super capacitors for the modern applications, as per their better charge storage capacity.

Capacitances of CP samples have been calculated from their peak areas [23] (Figure 6, Table 4). Sample S-C has shown with maximum and persistent capacitance (53 mC), on the contrary S-B has been found with least and volatile values (26 mC). Sample S-C has least crystallite size (Table 3), high surface functionalities (Figure 2) and least thermal stability (Figure 4, Table 2). Tiny morphology and tall surface functionalities have shaped sample S-C with distinctive electrochemical behavior in terms of charge storage capacity.

Table 4: Capacitance (mC) and Current capacity (Amp) values of prepared CP samples

Sample ID	mC_c	$Amp_c=C/s$	mC_a	$Amp_a=C/s$
S-A	36	1.26	11	0.76
S-B	26	0.94	9	0.67
S-C	53	1.85	19	1.24
S-D	31	1.11	10	0.70

Table 5: Carbon Particles CV results obtained at a scan rate of 25mV/s

Sample ID	I_{pc} (μA)	I_{pa} (μA)	I_{pa}/I_{pc}	ΔE_p
S-A	2.67	1.12	0.42	376.67
S-B	2.68	1.47	0.55	372.88
S-C	1.36	2.69	1.97	471.36
S-D	1.58	1.59	1.01	413.68

Sample S-C has the least positive peak current and S-B the highest (Table 5). The residual current of all CP (Table 5) at 25mV/s scan rate specify irreversibility of electrochemical reaction [24]. The result has also been confirmed by Ψ (surface electrical potential) values of all CP (Table 6), calculated by the formula:

$$\Psi = 1 / (nF/RT) \ nFA \times (\pi \ \alpha \ D_o)^{1/2} C_o R_u \ ^{[25]}$$

The change in electrochemical behavior of <mark>CP</mark> with time was studied by taking several scans of CV for all particles in 1M NaOH at a scan rate of 25mV/s (Figure 6). Charge/discharge study at 500 mA current supply showed a mirror-image relationship between the two segments, <mark>demonstrating least internal resistance(iR).</mark> <mark>Muted iR and capability to endure voltage (Figure 6), demonstrating permanency and reusability of the material, suggest sample S-D as a suitable candidate in electrochemical devices.</mark>
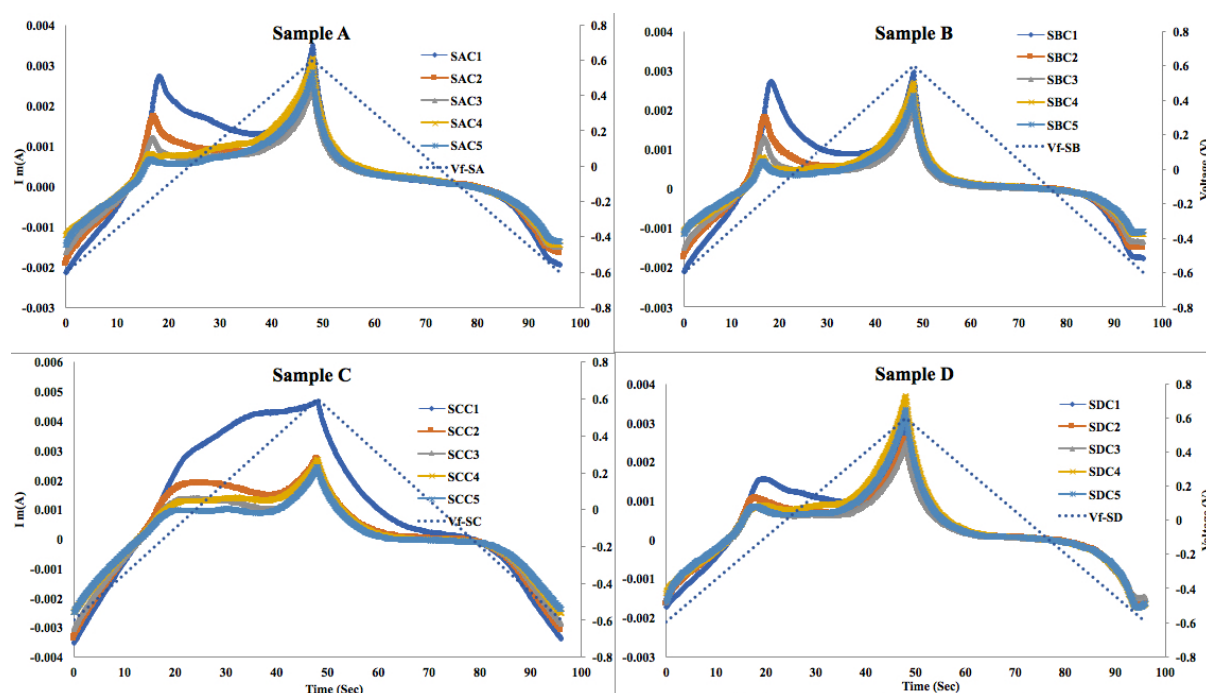

<mark>Figure 7:</mark> CV curves of <mark>CP</mark> at scan rate of 25mV/s in 1M NaOH, at different time intervals

Table 6: Electrochemical behavior of Carbon Particles

Sample ID	Ψ	ΔE_p x n (mV)	Electrochemical Area[a][24] (cm^2)
S-A	3.02 e-10	150.67	4.37
S-B	1.62 e-10	205.08	3.83
S-C	1.61 e-11	928.58	2.30
S-D	4.40 e-11	417.82	1.98

[a] calculated from formula A=(it$^{1/2}$)(p$^{1/2}$)/nFD$_o$$^{1/2}$C; where i=instantaneous current in amp, t=time in seconds, n=number of electrons involved, F=Faradays constant, D$_o$=Diffusion coefficient, C=molar concentration

<mark>Electrochemical capacitors for energy storage require excellent charge storage capacity (peak area analysis) as well as charge delivery (charge-discharge) response. Peak area analysis (Table 4) and charge-discharge study (Figure 7) of CP presented different charge storage capacities yet samples have been found with almost equivalent charge delivery response. Difference in</mark>

charge storage capacity might be due to difference in morphology, whereas equivalency in charge delivery response attributes to similarity in chemical nature.

CP have been tested for pH, conductivity and zeta potential values (Table 7). Basic pH has been witnessed for all CP indicating amide linkages. S-A has been found with highest basic pH (8.2) and highest zeta potential value (-28.6 mV), indicating the particle surface decorated with comparatively huge amount of charged species. This greater charge/ion concentration have made CP vulnerable towards fast electron transfer (CV results). Sample S-B has same basic pH (8.2) but comparatively lesser value of zeta potential (-20.9 mV) demonstrating lesser charged contents on the surface of CP, but larger conductivity value in solution (43.5 µS/cm) evidence higher polarizability because of charged contents within the particles. In contrast to these, sample S-C has zeta potential value (-24.6 mV) and conductivity (34.9 µS/cm) almost comparable to both S-A and S-B, yet it has shown less basic pH (7.9) than both. These findings prove different functionalities on CP surface, consequently changed electrochemical behavior.

Zeta potential of S-D (-17.4 mV) is least in all four CP, yet equals to that of Ref-CB (-17.5 mV), exhibiting the surfaces of both S-D and Commercial CB are equally decorated with charged species. A comparison of conductivity in solution reveals that S-D has better conductivity than commercial CB, which might be because of difference in quality and quantity of charged species within material layers as per less basic pH of S-D than Ref-CB (Table 4).

fTable 7: CP analyses for conductivity, pH and Zeta potential

Sample ID	ε	Conductivity (µS/cm)		ζ (mV)	pH
		Malvern Zeta	Conductometer		
Ref-CB	78.5	27.3	18.1	-17.5	8.3
S-A	78.5	29.5	20.2	-28.6	8.2
S-B	78.5	43.5	38.2	-20.9	8.2
S-C	78.5	34.9	22.1	-24.6	7.9
S-D	78.5	35.2	19.78	-17.4	7.8

Samples' conductivities have been tested through two different instruments, in solution form. The conductivity difference for the same sample (Table 7) obtained from two different instruments might be due to the difference in analysis capacity at a particular depth below sample surface.

Capacity of CP have been tested experimentally for the removal of metals (Pb and Zn) from water. Metal adsorption capacity of prepared CP has been tested by immersing CP in metal solutions, separately, for a day with constant stirring. After the specific time interval metal concentrations in solutions have been tested to find out the adsorbed quantities (Table 8, Fig 7).

Table 8: Lead and Zinc adsorption on CP

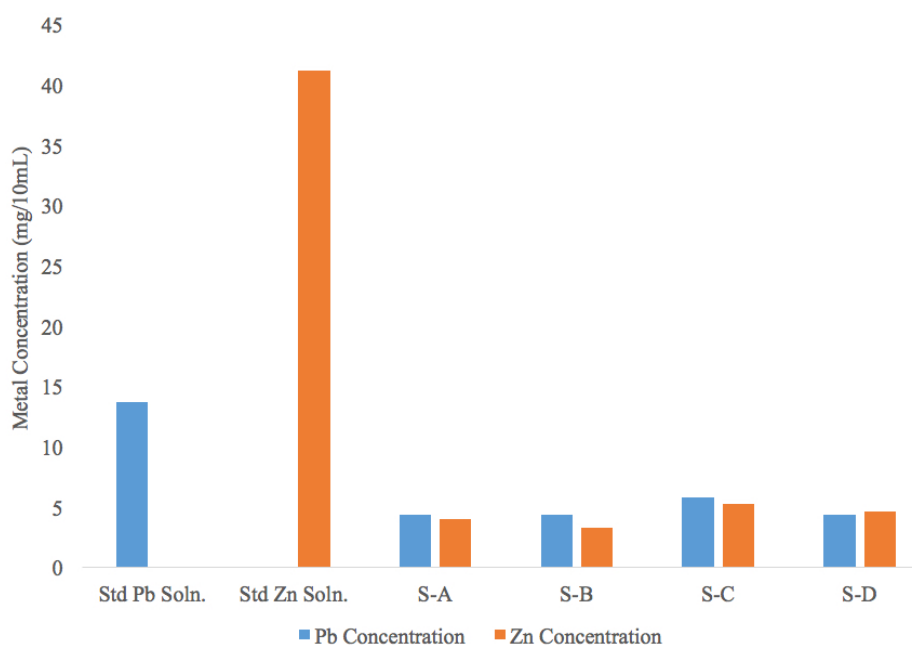| Sr. #	Sample ID	Pb (mg)		Adsorption (%)	Zn (mg)		Adsorption (%)
		In soln.	Adsorbed		In soln.	Adsorbed	
1	M-Blank	13.670	0.000	NA	41.19	0.00	NA
2	S-A	4.345	9.325	68.21	3.93	37.26	90.45
3	S-B	4.345	9.325	68.21	3.27	37.92	92.06
4	S-C	5.797	7.873	57.59	5.24	35.95	87.28
5	S-D	4.345	9.325	68.21	4.58	36.61	88.89

Figure 8: Metal adsorption on CP

Results have shown that higher concentration (90%) of Zn have been adsorbed by CP (Table 8, Figure 8). It may be attributed to self-sustained pH which facilitated easy electron transfer

mechanism as shown by CV analysis. Easily available electrons might have provided an anchor to metal cations in solution. Sample S-C as per its double layer capacitance and reduced electron transfer tendency (CV data) has shown least adsorption. The adsorption tendency of CP towards Pb has been found less i.e =68%.

CONCLUSION

Promoting recycling trend, this work has converted waste human hair into particles for conductive as well as adsorptive applications. Prepared samples have been found with speedy electron transfer mechanism, better charge storage and swift ionic diffusion along with their low cost and environmental compatibility, suggesting their potential utilization in renewable energy resources. The fast electron transfer mechanism has also facilitated the huge adsorption of metal cations on CP surface. These metal decorated CP may also lead to a wide range of applications.

ACKNOWLEDGEMENT

REFERENCES

1. Bhushan, B. Nanoscale characterization of human hair and hair conditioners. *Progress in Materials Science* **2008**, 53(4): 585-710.
2. Wu, X. L., Wen, T., Guo, H. L., Yang, S., Wang, X. and Xu, A. W. Biomass-derived sponge-like carbonaceous hydrogels and aerogels for supercapacitors. *ACS nano* **2013**, 7(4): 3589-3597.

3. Pramanick, B., Cadenas, L. B., Kim, D. M., Lee, W., Shim, Y., Martinez-Chapa, S. O., Madou, M. J. and Hwang, H. (2016). Human hair-derived hollow carbon microfibers for electrochemical sensing. *Carbon*, *107*, 872-877.

4. Hearle, J. A critical review of the structural mechanics of wool and hair fibers. *International journal of biological macromolecules* **2000***, 27*(2): 123-138.

5. Lee, L. D. and Howard, P. B. Chemistry and composition of the keratins. *International journal of dermatology* **1975**, 14(3): 161-171.

6. Rashaid, A. H. B., Peter B. H. and Glen P. J. Amino acid composition of human scalp hair as a biometric classifier and investigative lead. *Analytical Methods* **2015**, 7(5): 1707-1718.

7. Wufuer, R., Song, W., Zhang, D., Pan, X. and Gadd, G. M. A survey of uranium levels in urine and hair of people living in a coal mining area in Yili, Xinjiang, China. *Journal of environmental radioactivity* **2018**, 189: 168-174.

8. Gonçalves, A. L., José CM. P. and Manuel S. A review on the use of microalgal consortia for wastewater treatment. *Algal Research* **2017**, 24: 403-415.

9. Baltenneck, F., Garson, J. C., Engström, P., Riekel, C., Leroy, F., Franbourg, A. and Doucet, J. Study of the keratinization process in human hair follicle by X-ray micro-diffraction. *Cellular and molecular biology (Noisy-le-Grand, France)* **2000**, 46(5): 1017-1024.

10. Kumar, R., Tiwari, R. S. and Srivastava, O. N. Scalable synthesis of aligned carbon nanotubes bundles using green natural precursor: neem oil. *Nanoscale research letters* **2011**, 6(1): 92.

11. Gupta, A. Human hair waste and its utilization: gaps and possibilities. *Journal of waste management* **2014**, 498018: 1-17.

12. Dong, H., Zhang, H., Xu, Y. and Zhao, C. Facile synthesis of α-Fe_2O_3 nanoparticles on porous human hair-derived carbon as improved anode materials for lithium ion batteries. *Journal of Power Sources* **2015,** 300: 104-111.

13. Qian, W., Sun, F., Xu, Y., Qiu, L., Liu, C., Wang, S. and Yan, F. Human hair-derived carbon flakes for electrochemical supercapacitors. *Energy & Environmental Science* **2014,** 7(1): 379-386.

14. Kumar, R., Varshney, S., Kar, K. K. and Dasgupta, K. Enhanced thermo-mechanical and electrical properties of carbon-carbon composites using human hair derived carbon powder as reinforcing filler. *Advanced Powder Technology* **2018,** 29(6): 1417-1432.

15. Luo, F., Wu, K., Wang, S. and Lu, M. Melamine resin/graphite nanoflakes hybrids and its vacuum-assisted prepared epoxy composites with anisotropic thermal conductivity and improved flame retardancy. *Composites Science and Technology* **2017,** 144: 100-106.

16. Masaebi, N., Seyed, J. P., and Iraj, A. Electrically conductive nanocomposite adhesives based on epoxy resin filled with silver coated nanocarbon black. *Journal of Materials Science: Materials in Electronics* **2018,** 29(14): 11840-11851.

17. Zeng, C., Lu, S., Song, L., Xiao, X., Gao, J., Pan, L., Hea, Z. and Yu, J. Enhanced thermal properties in a hybrid graphene–alumina filler for epoxy composites. *RSC Advances* **2015,** 5(45): 35773-35782.

18. Skoog, D. A., West, D. M., Holler, F. J. and Crouch, S. R. Analytical Chemistry: An Introduction, 7th ed. Chapter 15, pp: 345-48

19. Zhao, Z.-Q., Xiao, P.-W. , Zhao, L., Liu, Y. and Han, B.-H. Human hair-derived nitrogen 1193 and sulfur co-doped porous carbon materials for gas adsorption, RSC Adv. 5 1194 (2015) 73980–73988. 1195.

20. Noeḿie, E., Kelley, J. R., Brian, D. M., Eric, S. R., Thomas T. E. and Jillian L. D. A Practical Beginner's Guide to Cyclic Voltammetry, J. Chem. Educ. 2018, 95, 197−206, DOI: 10.1021/acs.jchemed.7b00361.

21. Du, X., Wang, C., Chen, M., Jiao, Y. and Wang, J. Electrochemical Performances of Nanoparticle Fe3O4/Activated Carbon Supercapacitor Using KOH Electrolyte Solution. J. Phys. Chem. C **2009**, 113: 2643–2646.

22. Du, X., Wei Zhao, W., Wang, Y., Wang, C., Chen, M., Qi, T., Hua, C. and Ma, M. Preparation of activated carbon hollow fibers from ramie at low temperature for electric double-layer capacitor applications. *Bioresource Technology* **2013**, 149: 31-37.

23. Wang, H., Hao, Q., Yang, X., Lu, L., and Wang, X. A nanostructured graphene/polyaniline hybrid material for supercapacitors. *Nanoscale*, **2010**, 2(10): 2164-2170.

24. Shui, X., Frysz, C.A. and Chung D. D. L. Solvent cleansing of the surface of carbon filaments and its benifit to the electrochemical behavior. *Carbon* **1995**, 33(12): 1681-1698

25. Nicholson, R. S. Theory and application of cyclic voltammetry for measurement of electrode reaction kinetics. *Analytical chemistry* **1965** *37*(11): 1351-1355.